Chinese Chemical Letters 37 (2026) 111037

Contents lists available at ScienceDirect

Chinese Chemical Letters

journal homepage: www.elsevier.com/locate/cclet

Nanoscale design and composite engineering on RuO_2 cathode for high-performance zinc-ion hybrid capacitors

Yi Zhang[a], Meiyan Wang[a], Yirong Zhu[a,*], Junjun Yao[a], Rui Zhao[a], Wenbo Wang[b,*]

[a] College of Materials and Advanced Manufacturing, Hunan University of Technology, Zhuzhou 412007, China
[b] College of Materials Science and Engineering, Hunan Institute of Technology, Hengyang 421002, China

ARTICLE INFO

Article history:
Received 4 December 2024
Revised 24 February 2025
Accepted 5 March 2025
Available online 5 March 2025

Keywords:
RuO_2 nanodots
Reduced graphene oxide
Pseudocapacitive cathode
Zinc-ion hybrid capacitors
Energy storage mechanism

ABSTRACT

The design and exploitation of high-property cathode materials and the exploration of their energy storage mechanism have always been research hotspots in the area of zinc-ion hybrid capacitors (ZHCs). In this study, the new RuO_2 nanodots/reduced graphene oxide (RuO_2 NDs/rGO) composite is designed, and employed as a cathode for ZHC for the first time. Thanks to the synergism of nanoscale design and composite engineering, the RuO_2 NDs/rGO//Zn ZHC delivers large specific capacitance (169.5 mAh/g at 0.1 A/g), splendid rate property (74.4 mAh/g at 20 A/g), eminent cyclic property (up to 10,000 cycles), and high energy and power densities (101.7 Wh/kg and 12 kW/kg). Furthermore, systematic kinetic analyses are used to confirm the rapid ion transport kinetics of the RuO_2 NDs/rGO//Zn ZHC. More importantly, systematic ex-situ measurements are employed to illustrate its energy storage mechanism of the coexistence of electric double-layer capacitance (physical adsorption/desorption of SO_4^{2-}) and pseudocapacitance (insertion/extraction of Zn^{2+} and H^+ and chemical adsorption/desorption between Zn^{2+} and oxygen-containing functional groups). This study not only offers a good strategy for the design and exploitation of high-performance pseudocapacitive cathode for ZHCs, but also proposes an insight into energy storage mechanism of RuO_2-based pseudocapacitive cathode.

© 2026 Published by Elsevier B.V. on behalf of Chinese Chemical Society and Institute of Materia Medica, Chinese Academy of Medical Sciences.

Recently, with the rapid development of consumer electronics, electric vehicles, and new energy systems, the requirement for high-property energy storage equipment has shown explosive growth [1,2]. Among them, Li-ion batteries (LIBs) have become the most extensively utilized commercial energy storage systems on account of their high energy density and high energy efficiency. However, the scarcity of lithium resources and safety problems have severely limited their further exploitation and application [3,4]. Among the new energy storage systems, aqueous Zn-ion hybrid capacitors (ZHCs) have drawn extensive concern from researchers owing to their large theoretical capacity (820 mAh/g), splendid stability, and low redox potential (−0.76 V *vs.* SHE) [5,6]. Unfortunately, the relatively small energy density of ZHCs impedes their practical applications. Generally, the zinc anodes have high theoretical specific capacitance, while the capacitive cathode materials have lower specific capacitance. According to the short-board effect, the design and development of high-capacitance cathode materials are crucial for boosting the energy density of ZHCs.

Carbon-based capacitive cathode materials, including porous carbon [7,8], activated carbon [9], carbon nanotubes [10], metal organic framework (MOF) derived carbon [11–13], and graphene [14–16], have been widely applied in ZHCs. Among them, researchers have modified carbon-based materials through strategies such as structural design and surface modification, which significantly improve their specific surface area, electronic conductivity and electrochemical reactivity, shorten their ion transport paths, and effectively improve their electrochemical performance [17,18]. However, the ZHCs with carbon-based cathode [19] still exhibit limited energy density arising from the energy storage process dominated by the electric double-layer (EDL) capacitance. In view of this, the exploitation of pseudocapacitive cathode materials with large theoretical specific capacitance is a good strategy to further boost the energy density of ZHCs.

Various typical pseudocapacitive cathode materials, including MXenes [20,21], conductive polymers [22], and transition metal oxides [23], exhibit higher theoretical specific capacitance due to their unique Faradaic reaction mechanisms. These materials are able to undergo reversible redox reactions with zinc ions, thereby storing more charge and enhancing the energy density of ZHCs. Among various pseudocapacitive cathode materials, RuO_2,

* Corresponding authors.
E-mail addresses: zhuyirong@hut.edu.cn (Y. Zhu), wenbohuit1982@163.com (W. Wang).

https://doi.org/10.1016/j.cclet.2025.111037
1001-8417/© 2026 Published by Elsevier B.V. on behalf of Chinese Chemical Society and Institute of Materia Medica, Chinese Academy of Medical Sciences.

especially hydrated amorphous RuO_2, is regarded as an ideal energy storage material due to its large theoretical specific capacitance, splendid stability, and highly reversible electrochemical oxidation/reduction characteristics compared with other cathode materials [23]. Unfortunately, the insufficient electrochemical reaction between RuO_2 and the electrolyte results in limited specific capacitance, as well as poor rate performance and cyclic lifespan. The RuO_2 nanomaterials have been proved to have the characteristics of small particle size and high surface/volume ratio, which can sufficiently improve the utilization of electrode materials and enhance their electrochemical redox behavior [24]. However, the high surface energy of nanomaterials can cause severe agglomeration, resulting in the inhomogeneity and densification of morphology and structure, thereby seriously affecting their electrochemical performance. The combination of RuO_2 nanomaterials and reduced graphene oxide (rGO) is a feasible method to prevent their agglomeration [25]. The introduction of rGO can reduce the proportion of RuO_2 in the composite, consequently decreasing its cost. Moreover, rGO has excellent electronic conductivity and can be used as a conductive matrix to boost the conductivity and electrochemical reactivity of RuO_2, thus boosting the overall electrochemical performance of the composite. Therefore, the construction of RuO_2 nanodots (NDs)/rGO composite is a feasible strategy to achieve efficient energy storage of ZHCs. As we know, there is no study on the application of RuO_2 NDs/rGO in ZHCs, and its energy storage mechanism of RuO_2-based pseudocapacitive cathode materials in ZHCs has not been reported yet. Therefore, it is highly significant to study the electrochemical behavior and energy storage mechanism of the RuO_2 NDs/rGO cathode in ZHCs.

In this work, the new RuO_2 NDs/rGO composite was prepared through sol-gel method combined with low-temperature anneal treatment, and utilized as a cathode for ZHC for the first time. Thanks to the synergism of nanoscale design and composite engineering, the assembled RuO_2 NDs/rGO//Zn ZHCs based on the RuO_2 NDs/rGO cathode exhibits large specific capacitance (169.5 mAh/g at 0.1 A/g), superior rate property (74.4 mAh/g at 20 A/g), remarkable cyclic performance (90.4 % capacity retention after 10,000 cycles at 5 A/g), large energy and power densities (101.7 Wh/kg at 60 W/kg and 41.7 Wh/kg at 12 kW/kg). More impressively, the energy storage mechanism of the EDL and pseudocapacitive reactions of electrolyte ions in the RuO_2 NDs/rGO cathode was elucidated for the first time through electrochemical kinetic analyses based on kinetic analyses (cyclic voltammetry (CV) and electrochemical impedance spectroscopy (EIS)) and systematic *ex-situ* tests (X-ray diffraction (XRD), field emission scanning electron microscopy (FESEM) and corresponding energy-dispersive X-ray spectroscopy (EDS), EIS, and X-ray photoelectron spectroscopy (XPS)). This research not only affords a good strategy for the design and development of ZHCs pseudocapacitive cathode, but also elucidates the energy storage mechanism of the RuO_2 NDs/rGO cathode for the first time.

The synthesis process of the RuO_2 NDs/rGO composite is presented in Fig. 1a. The RuO_2 NDs/rGO composite was prepared by sol-gel method combined with low-temperature calcination treatment using $RuCl_3{\cdot}nH_2O$ and GO as precursors. The morphology, microstructure and elemental composition and distribution of the prepared RuO_2 NDs/rGO composite were evaluated by FESEM, (high-resolution) transmission electron microscopy (TEM/HRTEM) and elemental mapping tests. As presented in the FESEM images, compared with the agglomerated pure RuO_2 (Fig. 1b and Fig. S1 in Supporting information), the RuO_2 NDs/rGO composite presents a rGO sheet structure with some folds and the presence of uniformly distributed RuO_2 nanodots on the rGO sheet structure (Fig. 1c and Fig. S2 in Supporting information). By the further TEM test (Fig. 1d), it is observable that the RuO_2 nanodots are even distributed on the rGO sheets with a size of 5–8 nm. As presented in the HRTEM image (Fig. 1e), a lattice spacing of 0.26 nm can be observed, belonging to the (101) crystal plane of RuO_2, which is consistent with XRD analysis results [26]. Moreover, the co-presence and uniform distribution of Ru, O, and C elements in the RuO_2 NDs/rGO composite are clearly observed in the elemental mapping test, as demonstrated in Fig. S3 (Supporting information). Besides, N_2 adsorption-desorption test (Fig. S4 in Supporting information) reveals that the RuO_2 NDs/rGO composite possesses a high BET surface area of 54.9 m^2/g and abundant mesopores in the range of 2.7–4.2 nm, which is conducive to zinc storage and fast ion transport.

In addition, the structure of the pure RuO_2 and RuO_2 NDs/rGO composite was examined by XRD test. As shown in Fig. 1f, it is clear that no strong characteristic peaks of RuO_2 crystal planes are observed, and two weak and broad diffraction peaks emerge at $2\theta = 32.9°$ and 56.2°, corresponding to the (101) and (220) planes of RuO_2, respectively, which indicates that the RuO_2 formed during the low-temperature annealing at 150 °C is typically amorphous [27,28]. The TG curves of the pure RuO_2 and RuO_2 NDs/rGO composite are shown in Fig. 1g, from which the mass percentage of rGO in the RuO_2 NDs/rGO composite is calculated to be approximately 10 wt%. In order to further investigate the elemental composition and chemical valence of the RuO_2 NDs/rGO composite, XPS test was executed. As manifested in Fig. 1h, the survey spectrum of the RuO_2 NDs/rGO composite confirms the existence of Ru, O, and C elements. In the high-resolution C 1s/Ru 3d spectrum (Fig. 1i), the peaks situated at 287.2, 284.8, 282.2, and 281.1 eV are indexed to the C–O-H, C–C, Ru $3d_{3/2}$, and Ru $3d_{5/2}$ [29,30], respectively, and the peak position of Ru $3d_{5/2}$ indicates the existence of Ru^{4+}, further verifying the successful preparation of RuO_2 [31]. Additionally, in the high-resolution Ru 3p spectrum (Fig. 1j), the main peaks situated at 484.8 and 462.6 eV match with Ru $3p_{1/2}$ and Ru $3p_{3/2}$, respectively, which belong to ruthenium (IV) oxide [26]. The high-resolution O 1s spectrum (Fig. 1k) shows three characteristic peaks at 532.1, 530.0, and 528.8 eV, which are relevant to bound water, Ru-O-H, and Ru-O-Ru, respectively [32,33].

The ZHC (denoted as rGO//Zn, RuO_2//Zn and RuO_2 NDs/rGO//Zn ZHC) was constructed utilizing Zn foil as the anode, rGO, RuO_2 and RuO_2 NDs/rGO as the cathode, and 2 mol/L $ZnSO_4$ solution as the electrolyte (Fig. 2a). Fig. S5 (Supporting information) displays the CV profiles of the RuO_2 NDs/rGO//Zn ZHC at different voltages, indicating that they can operate stably in the voltage range of 0.4–1.6 V. Figs. 2b and c compare the CV profiles (5 mV/s) and GCD profiles (0.3 A/g) of the rGO//Zn, RuO_2//Zn and RuO_2 NDs/rGO//Zn ZHCs. Compared with rGO//Zn and RuO_2//Zn ZHC, the RuO_2 NDs/rGO ZHC presents larger CV curve area and higher reversible specific capacity. As presented in Figs. 2d and e and Fig. S6 (Supporting information), all GCD curves are approximately symmetric at current densities of 0.1–20 A/g, indicating that the ZHCs have good capacitive behavior. The specific capacities of the RuO_2 NDs/rGO//Zn ZHC at current densities of 0.1, 0.2, 0.3, 0.5, 1, 2, 3, 5, 10, and 20 A/g are 169.5, 158.5, 153.2, 147.9, 141.4, 133.0, 126.1, 114.7, 95.0, and 74.4 mAh/g, respectively, exhibiting larger specific capacity and better rate performance compared to rGO//Zn and RuO_2//Zn ZHC (Fig. 2f), which is ascribed to the synergism of nanoscale design and composite engineering on the RuO_2 cathode [34]. It is worth noting that the RuO_2 NDs/rGO//Zn ZHC exhibits an energy density of 101.7 Wh/kg @60 W/kg based on the RuO_2 NDs/rGO cathode, and still retains an energy density of 44.7 Wh/kg even at 12 kW/kg, outperforming most of previously reported ZHCs such as GH//Zn (76.2 Wh/kg @147.6 W/kg, 39 Wh/kg @6.54 kW/kg) [35], AC//Zn (84 Wh/kg @66.6 W/kg, 30 Wh/kg @14.9 kW/kg) [9], ACC//Zn (100 Wh/kg @43.9 W/kg, 20.4 Wh/kg @1.69 kW/kg) [36], EG/PANI//POP-TAPP-NTCA (48 Wh/kg @85 W/kg, 12 Wh/kg @2.01 kW/kg) [37], NPC//Zn (82 Wh/kg @167.7 W/kg, 35 Wh/kg @12.5 kW/kg) [38],

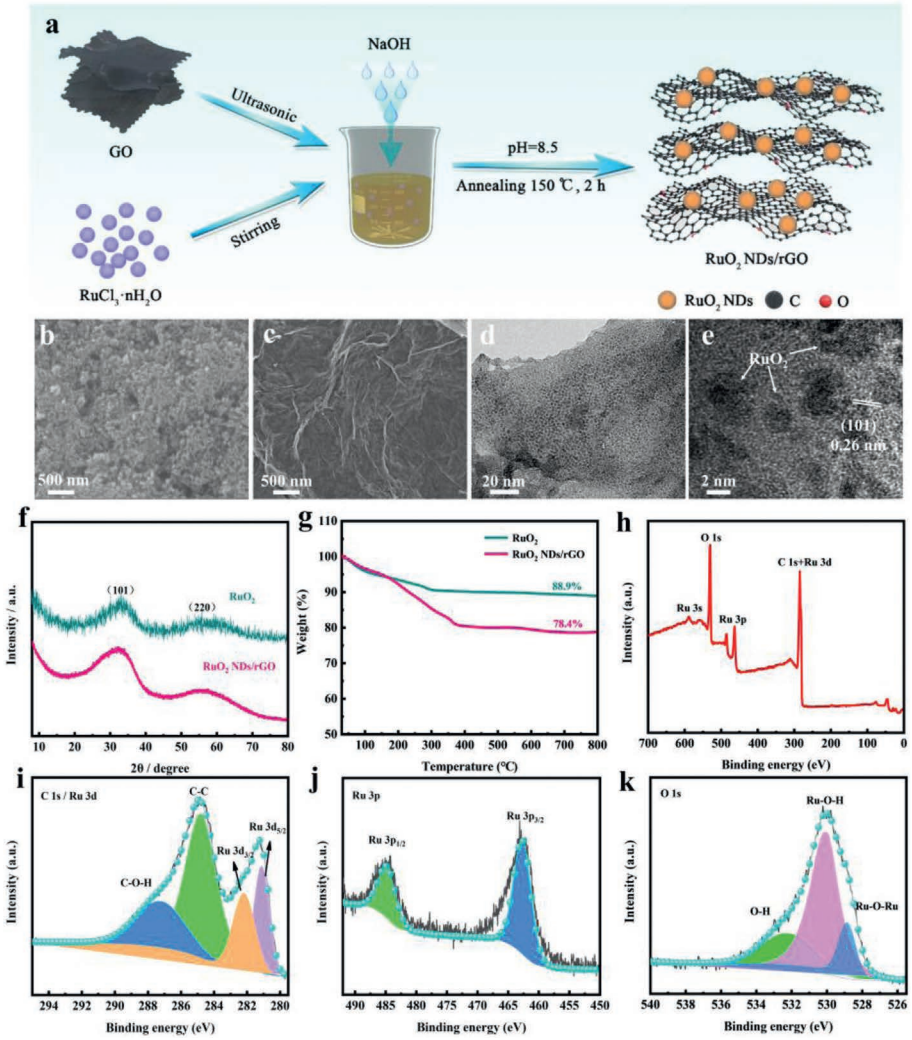


Fig. 1. (a) Schematic diagram of the synthesis process of the RuO_2 NDs/rGO composite. FESEM images of the (b) pure RuO_2 and (c) RuO_2 NDs/rGO composite. (d) TEM and (e) HRTEM images of the RuO_2 NDs/rGO composite. (f) XRD patterns and (g) TG curves of the pure RuO_2 and RuO_2 NDs/rGO composite. (h) XPS full spectrum and high-resolution (i) C 1s/Ru 3d, (j) Ru 3p, and (k) O 1s XPS spectra of the RuO_2 NDs/rGO composite.

N,P-MXene//Zn (43.9 Wh/kg @117 W/kg, 19 Wh/kg @29 kW/kg) [39], and H-MXene//Zn (53.6 Wh/kg @110 W/kg, 28 Wh/kg @2.3 kW/kg) [40], as presented in Fig. 2g. Fig. 2h exhibits a small fan powered by two RuO_2 NDs/rGO//Zn ZHCs in series, confirming their potential practical application, which further indicates their superior energy storage property. In addition, the cycling performance of the RuO_2 NDs/rGO//Zn ZHC was tested at 5 A/g (Fig. 2i). The capacity retention of the RuO_2 NDs/rGO//Zn ZHC reaches up to 90.4 % after 10,000 charge-discharge cycles, and its coulombic efficiency approaches 100 % during the cycling process, demonstrating its remarkable cycling stability and reversibility.

The electrochemical kinetic performance of the RuO_2//Zn and RuO_2 NDs/rGO//Zn ZHCs was compared by EIS and CV tests. As exhibited in the EIS spectra (Fig. 3a), the RuO_2 NDs/rGO//Zn ZHC presents a smaller internal resistance (R_s, 0.84 Ω) and charge transfer resistance (R_{ct}, 63.9 Ω) than the RuO_2 electrode by fitting the equivalent circuit diagram, confirming its faster charge transfer kinetics. Meanwhile, Fig. 3b presents the linear fitting diagram of Z' *vs.* $\omega^{-1/2}$ in the low-frequency region, and the fitted Warburg coefficients (σ) are 11.1 (the RuO_2 NDs/rGO//Zn ZHC) and 17.9 (the RuO_2//Zn ZHC), respectively. Based on this, the calculated diffusion coefficient of the RuO_2 NDs/rGO//Zn ZHC (4.36×10^{-12} cm^2/s) is higher than that of the RuO_2//Zn ZHC (1.68×10^{-12} cm^2/s), which exhibits the same level of ion diffusion capability as supercapacitors, confirming its excellent ion diffusion kinetics [41]. Figs. 3c and d show the CV profiles of the RuO_2//Zn and RuO_2 NDs/rGO//Zn ZHCs in the voltage range of 0.4–1.6 V at sweep rates varying from 2 mV/s to 100 mV/s, and a pair of wider redox peaks in the CV profiles are clearly observed. It is noteworthy that the redox peaks still exist at a high sweep rate of 100 mV/s, implying that the RuO_2 NDs/rGO//Zn ZHC has a good rate property. Furthermore, the electrolyte ion diffusion coefficient can be obtained by fitting the linear relationship between the peak current (I_p) and the sweep rate ($v^{1/2}$) [42–44], as manifested in Fig. 3e. The calculated ion diffusion coefficient of the oxidation and reduction peaks is 7.58×10^{-12} and 4.51×10^{-12} cm^2/s, respectively, which is consistent with the EIS kinetic analysis, further confirming the excellent ion diffusion kinetics of the RuO_2 NDs/rGO//Zn ZHC. Furthermore, the excellent electrochemical reaction kinetics of the RuO_2 NDs/rGO//Zn ZHC was further elucidated by a semi-qualitative analysis of the linear relationship between the peak current (I_p) and the sweep rate (v) [42–44]. As demonstrated in Fig. 3f, the fitted *b*-value of the oxidation and reduction peaks of the RuO_2 NDs/rGO//Zn ZHC is 0.86 and 0.83, respectively, which is higher than that of the RuO_2 electrode (0.80 and 0.79), indicating the more surface capacitive behavior and better electrochemical kinetics. Moreover, as shown

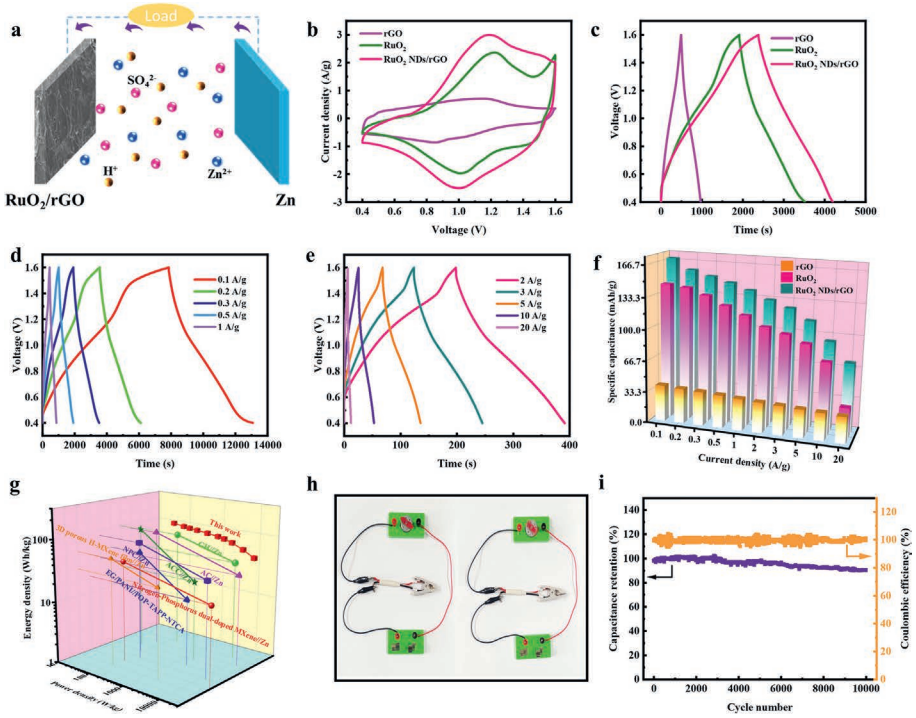


Fig. 2. (a) Configuration of the RuO_2 NDs/rGO//Zn ZHC. (b) CV profiles at 5 mV/s and (c) GCD profiles at 0.3 A/g of the rGO//Zn, RuO_2//Zn and RuO_2 NDs/rGO//Zn ZHCs. (d, e) GCD profiles at various current densities of the RuO_2 NDs/rGO//Zn ZHC. (f) Rate capability of the rGO//Zn, RuO_2//Zn and RuO_2 NDs/rGO//Zn ZHCs. (g) Ragone plot of the RuO_2 NDs/rGO//Zn ZHC in contrast with other ZHCs. (h) Digital images of a small fan driven by two ZHCs. (i) Cycle property and Coulombic efficiency of the RuO_2 NDs/rGO//Zn ZHC after 10,000 cycles at 5 A/g.

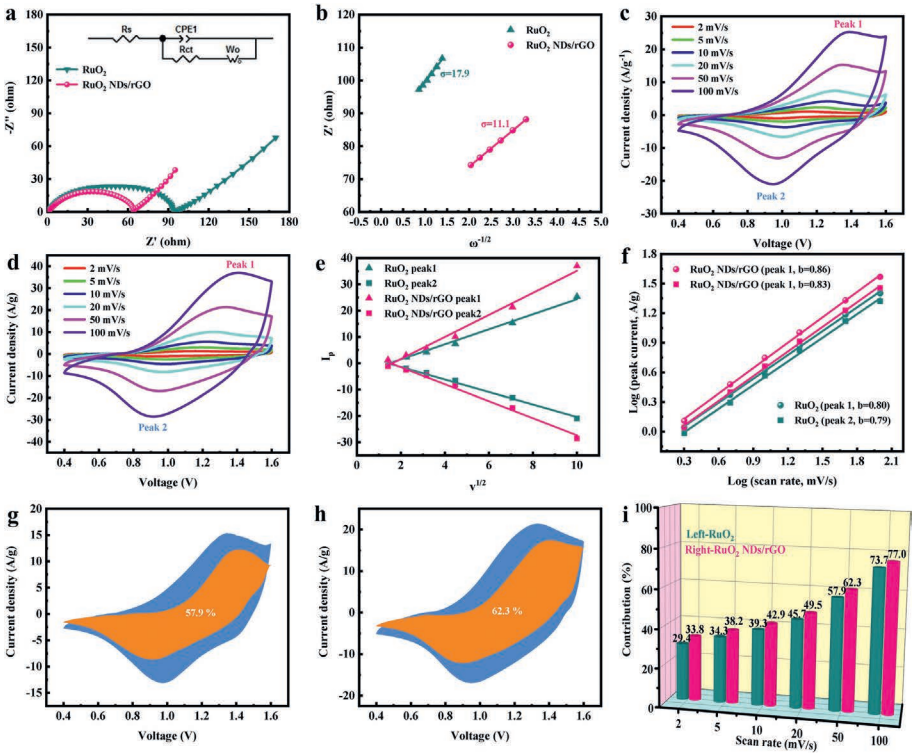


Fig. 3. (a) EIS plot, (b) linear fitting of Z' *vs.* $\omega^{-1/2}$ plot in the low-frequency region, (c, d) CV curves at various sweep rates, (e) the linear relationship between I_p and $v^{1/2}$, (f) LogI_p *vs.* log*v* plots, (g, h) capacitive contribution at 20 mV/s and (i) capacitive contribution ratio at diverse sweep rates of the RuO_2//Zn and RuO_2 NDs/rGO//Zn ZHCs.

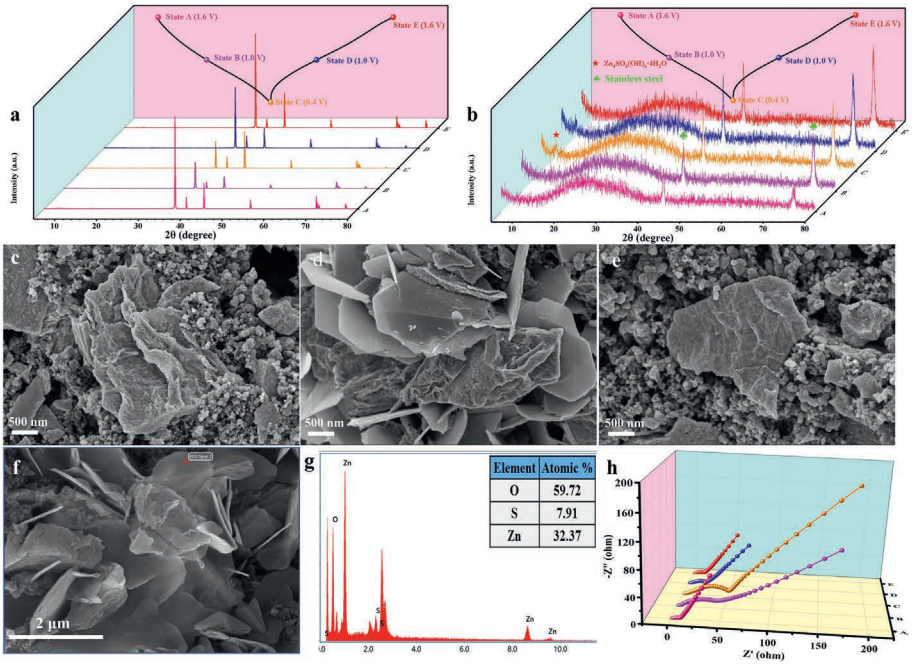


Fig. 4. *Ex-situ* XRD patterns of the (a) Zn anode and (b) RuO_2 NDs/rGO cathode at various states and corresponding GCD curves at 1 A/g, (c-e) *ex-situ* FESEM images at different states, (f) *ex-situ* FESEM image at fully discharged state and (g) corresponding EDS spectrum, and (h) EIS plots at different states of the RuO_2 NDs/rGO//Zn ZHC.

in Figs. 3g-i, the RuO_2 NDs/rGO//Zn ZHC exhibits higher capacitive contributions at various scan rates compared with the RuO_2 electrode, indicating the faster electrochemical kinetics and enhanced rate capability of the RuO_2 NDs/rGO electrode.

To explore the charge storage mechanism of the RuO_2 NDs/rGO//Zn ZHC, various *ex-situ* tests (XRD, FESEM, EIS, and XPS) were executed on the RuO_2 NDs/rGO cathode and Zn anode at diverse states during the charge-discharge process. As manifested in Fig. 4a, the RuO_2 NDs/rGO//Zn ZHC was first charged to 1.6 V (State A), and subsequently discharged to 1.0 V (State B) and 0.4 V (State C), followed by recharging to 1.0 V (State D) and 1.6 V (State E). During the charging and discharging process, the *ex-situ* XRD patterns of the Zn anode show no additional diffraction peaks of other substances, except for variations in the intensity of a few diffraction peaks, indicating that only the electrochemical reaction of Zn^{2+} deposition/stripping occurs on the anode. For the *ex-situ* XRD patterns of the cathode (Fig. 4b), it is observable that the main peak position of the RuO_2 NDs/rGO cathode does not change significantly during the electrochemical reaction, which indicates that the energy storage of the cathode is attributed to the insertion/extraction (or adsorption/desorption) of electrolyte ions. Meanwhile, it is observable that $Zn_4SO_4(OH)_6{\cdot}4H_2O$ (PDF #44–0673) is formed during the charge/discharge process [45]. The intensity of its characteristic peaks reaches its maximum at fully discharged state (State C), and subsequently disappears after recharging back to State E (1.6 V), suggesting a reversible precipitation/dissolution process. Furthermore, the formation and dissolution of sheet-like substances during the charging/discharging process are also directly observed by *ex-situ* FESEM images (Figs. 4c-e), and the corresponding EDS (Figs. 4f and g) test reveals that the ratio of Zn and S elements in this product is about 4:1, which further confirms the generation of $Zn_4SO_4(OH)_6{\cdot}4H_2O$. It is worth noting that the generation of $Zn_4SO_4(OH)_6{\cdot}4H_2O$ contributes less to the energy storage, and its formation is mainly related to the change of H^+/OH^- on the surface of the RuO_2 NDs/rGO cathode [46], implying that H^+ or OH^- is also involved in the reaction process besides the adsorption/desorption of SO_4^{2-} on the cathode contributing to the EDL capacitance. In addition, as shown in Fig. 4h, the *ex-situ* EIS test indicates that R_{ct} gradually increases during the discharge process and decreases during the subsequent charge process, further confirming the reversibility of the precipitation/dissolution process of $Zn_4SO_4(OH)_6{\cdot}4H_2O$.

To acquire a deeper comprehension of the ion storage mechanism on the RuO_2 NDs/rGO//Zn ZHC, *ex-situ* XPS characterization was further employed to investigate the changes in surface chemical composition of the electrode at various states. As manifested in Fig. 5a, the high-resolution Zn 2p spectra show that the electrode has a strong Zn characteristic peak at State C, which arises from the generation of $Zn_4SO_4(OH)_6{\cdot}4H_2O$ and the insertion of Zn^{2+} during the discharge process [47]. After charging to State E, the intensity of characteristic peak of $Zn_4SO_4(OH)_6{\cdot}4H_2O$ is significantly weakened arising from the dissolution of $Zn_4SO_4(OH)_6{\cdot}4H_2O$ and the extraction of most Zn^{2+}. The insertion of Zn^{2+} is further confirmed in the high-resolution Ru 3p spectra (Fig. 5b), and a new Zn characteristic peak appears upon discharging to State C, which is significantly weakened upon recharging to State E, again confirming the possible pseudocapacitive reaction due to the insertion/extraction of Zn^{2+} on RuO_2. As manifested in the high-resolution C 1s spectra (Fig. 5c), the presence of the characteristic peak of C–O-Zn is detected during the charging and discharging process, confirming the presence of chemical adsorption and desorption reactions between Zn^{2+} and the oxygen-containing functional groups of rGO, which contributes to a certain amount of pseudocapacitance [48]. As presented in the high-resolution O 1s spectra (Fig. 5d), compared with the initial State A, the characteristic peak of Ru-O-H is significantly enhanced at fully discharged state, and returns to its initial level at fully charged state, which can be attributed to the pseudocapacitance generated by the H^+ insertion/extraction during the charging/discharging process, resulting in the improved specific capacitance of the electrode. In summary, the energy storage mechanism of the RuO_2 NDs/rGO//Zn ZHC is shown in Fig. 5e.

In summary, the RuO_2 NDs/rGO composite is prepared by sol-gel method combined with low-temperature calcination treatment, and utilized as a cathode for ZHC. Thanks to the synergistic effect of nanoscale design and composite engineering, the RuO_2

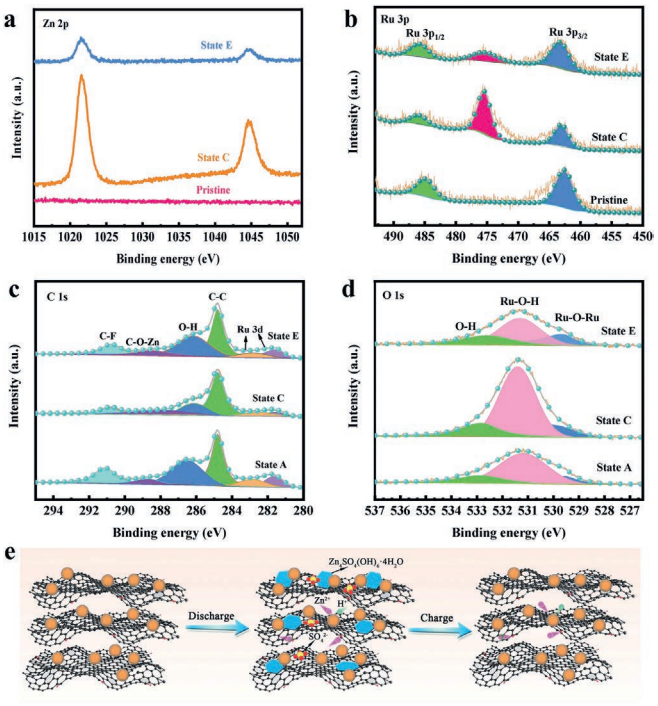


Fig. 5. *Ex-situ* high-resolution (a) Zn 2p, (b) Ru 3p, (c) C 1s, and (d) O 1s spectra at pristine, State C, and State E of the RuO_2 NDs/rGO//Zn ZHC. (e) Schematic representation of the energy storage mechanism of the RuO_2 NDs/rGO//Zn ZHC.

NDs/rGO//Zn ZHC achieves large specific capacitance (169.5 mAh/g at 0.1 A/g), excellent rate property (74.4 mAh/g at 20 A/g), long cyclic property (90.4 % capacity retention after 10,000 cycles at 5 A/g), and maximum energy and power densities (101.7 Wh/kg at 60 W/kg and 41.7 Wh/kg at 12 kW/kg). Moreover, systematic kinetic analyses based on CV and EIS tests elucidate the boosted ion transport kinetics of the RuO_2 NDs/rGO//Zn ZHC compared with the RuO_2//Zn ZHC. More encouragingly, systematic *ex-situ* XRD, FE-SEM, EDS, EIS, and XPS tests are utilized to reveal the energy storage mechanism of the EDL and pseudocapacitive reactions of electrolyte ions in the RuO_2 NDs/rGO cathode. This study provides a good strategy for the design and exploitation of high-performance ZHCs pseudocapacitive composite cathode and reveals the energy storage mechanism of RuO_2-based pseudocapacitive cathode for the first time.

Declaration of competing interest

The authors declare that they have no known competing financial interests or personal relationships that could have appeared to influence the work reported in this paper.

CRediT authorship contribution statement

Yi Zhang: Writing – original draft, Formal analysis, Data curation. **Meiyan Wang:** Writing – original draft, Formal analysis. **Yirong Zhu:** Writing – review & editing, Supervision, Resources, Project administration, Funding acquisition, Conceptualization. **Junjun Yao:** Methodology, Investigation, Data curation. **Rui Zhao:** Visualization, Validation, Software. **Wenbo Wang:** Writing – review & editing.

Acknowledgments

The work is financially supported by Distinguished Young Scientists of Hunan Province (No. 2022JJ10024), National Natural Science Foundation of China (No. 21601057), and Key Projects of Hunan Provincial Education Department (No. 22A0412).

Supplementary materials

Supplementary material associated with this article can be found, in the online version, at doi:10.1016/j.cclet.2025.111037.

References

[1] L. Cao, D. Li, T. Pollard, et al., Nat. Nanotechnol. 16 (2021) 902–910.
[2] J. Chen, Y. Liu, B. Xiao, et al., Angew. Chem. Int. Ed. 136 (2024) e202408667.
[3] C. Liu, Z. Song, X. Deng, et al., Chin. Chem. Lett. 35 (2024) 109081.
[4] R. Zhao, C. Liu, Y. Zhu, et al., Adv. Funct. Mater. 34 (2024) 2316643.
[5] H. Tang, J.J. Yao, Y.R. Zhu, et al., Adv. Energy Mater. 11 (2021) 2003994.
[6] J. Zhou, Q. Li, X. Hu, et al., Chin. Chem. Lett. 35 (2024) 109143.
[7] J. He, G. Peng, Y. Wei, et al., J. Power Sources 613 (2024) 234937.
[8] J. Yin, W.L. Zhang, W.X. Wang, et al., Adv. Energy Mater. 10 (2020) 2001705.
[9] L.B. Dong, X.P. Ma, Y. Li, et al., Energy Storage Mater. 13 (2018) 96–102.
[10] G.Q. Sun, H.S. Yang, G.F. Zhang, et al., Energy Environ. Sci. 11 (2018) 3367–3374.
[11] D. Jia, Z. Shen, Y. Lv, et al., Adv. Funct. Mater. 34 (2024) 2308319.
[12] D. Jia, Z. Shen, W. Zhou, et al., Chem. Eng. J. 485 (2024) 149820.
[13] T. Xiong, Y.R. Shen, W.S.V. Lee, et al., Nano Mater. Sci. 2 (2020) 159–163.
[14] J.R. Luo, L. Xu, H.M. Liu, et al., Adv. Funct. Mater. 32 (2022) 2112151.
[15] J. Yao, F. Li, R. Zhou, et al., Chin. Chem. Lett. 35 (2024) 108354.
[16] J.J. Yao, C. Liu, J.Y. Li, et al., Rare Met. 42 (2023) 2307–2323.
[17] Z.D. Huang, T.R. Wang, H. Song, et al., Angew. Chem. Int. Ed. 60 (2021) 1011–1021.
[18] J.Y. Li, X.R. Yun, Z.L. Hu, et al., J. Mater. Chem. A 7 (2019) 26311–26325.
[19] H. Li, X. He, T. Wu, et al., Fuel. Process. Technol. 230 (2022) 107203.
[20] K. Nasrin, V. Sudharshan, K. Subramani, et al., Adv. Funct. Mater. 32 (2022) 2110267.
[21] Q. Wang, S.L. Wang, X.H. Guo, et al., Adv. Electron. Mater. 5 (2019) 1900537.
[22] J.W. Han, K. Wang, W.H. Li, et al., Nanoscale 10 (2018) 13083–13091.
[23] L.B. Dong, W. Yang, W. Yang, et al., Nano-Micro Lett. 11 (2019) 94.
[24] Y. Zhu, X. Ji, C. Pan, et al., Energy Environ. Sci. 6 (2013) 6365-3675.
[25] S. Xie, Y. Li, X. Li, et al., Nano-Micro Lett. 14 (2021) 39.
[26] C.F. Zhang, Y.B. Xie, M.Q. Zhao, et al., ACS Appl. Mater. Interf. 6 (2014) 9751–9759.
[27] S.Y. Kong, K. Cheng, T. Ouyang, et al., Electrochim. Acta 246 (2017) 433–442.
[28] K.P. Xie, W. Xia, J. Masa, et al., J. Energy Chem. 25 (2016) 282–288.
[29] Z. Zhou, Y.R. Zhu, Z.B. Wu, et al., RSC Adv. 4 (2014) 6927–6932.
[30] M.Y. Chung, C.T. Lo, et al., Electrochim. Acta 364 (2020) 137324.
[31] H.T. Fang, M. Liu, D.W. Wang, et al., Nano Energy 2 (2013) 1232–1241.
[32] P.F. Wang, H. Liu, Q.Q. Tan, et al., RSC Adv. 4 (2014) 42839–42845.
[33] L.F. Wang, Y. Ding, J.Y. Li, et al., J. Electroanal. Chem. 919 (2022) 116501.
[34] C. Zhu, H. Liang, P. Li, et al., J. Energy Chem. 100 (2025) 637–645.
[35] Y.C. Zhu, X.K. Ye, H.D. Jiang, et al., J. Power Sources 453 (2020) 227851.
[36] K.A. Owusu, X. Pan, R. Yu, et al., Mater. Today Energy 18 (2020) 100529.
[37] F.Z. Cui, Z.C. Liu, D.L. Ma, et al., Chem. Eng. J. 405 (2021) 127038.
[38] X. Shi, H.Z. Zhang, S.Q. Zeng, et al., ACS Mater. Lett. 3 (2021) 1291–1299.
[39] Z. Li, D. Wang, Z. Sun, et al., Electrochim. Acta 455 (2023) 142440.
[40] F. Li, Y.L. Liu, G.G. Wang, et al., Chem. Eng. J. 435 (2022) 135052.
[41] Z.H. Lu, Z.L. Hu, L. Xiao, et al., Chem. Eng. J. 450 (2022) 138347.
[42] Y. Zhu, W. Zhong, W. Chen, et al., Nano Energy 125 (2024) 109524.
[43] X. Liu, Y. Zhu, Z. Lu, et al., Carbon Neutraliz. 2 (2023) 721–737.
[44] W. Zhong, R. Zhao, Y. Zhu, et al., Adv. Funct. Mater. 34 (2024) 2419720.
[45] H.Z. Zhang, Q.Y. Liu, Y.B. Fang, et al., Adv. Mater. 31 (2019) 1904948.
[46] X.Y. Deng, J.J. Li, Z. Shan, et al., J. Mater. Chem. A 8 (2020) 11617–11625.
[47] Q. Guo, J.J. Liu, C.C. Bai, et al., ACS Nano 15 (2021) 16533–16541.
[48] Y.Y. Shao, Z.T. Sun, Z.N. Tian, et al., Adv. Funct. Mater. 31 (2021) 2007843.